Intra-leaf modeling of *Cannabis* leaflet shape produces leaf models that predict genetic and developmental identities

Manica Balant [1,2,3], Teresa Garnatje [1,4], Daniel Vitales [1], Oriane Hidalgo [1,5], Daniel H. Chitwood [3,6]

[1] Institut Botànic de Barcelona, IBB (CSIC-CMCNB), Passeig del Migdia s.n., 08038 Barcelona, Spain

[2] Laboratori de Botànica (UB), Unitat Associada al CSIC, Facultat de Farmàcia i Ciències de l'Alimentació, Universitat de Barcelona, Av. Joan XXIII 27–31, 08028 Barcelona, Spain

[3] Department of Horticulture, Michigan State University, East Lansing, MI, USA

[4] Jardí Botànic Marimurtra - Fundació Carl Faust, pg. Carles Faust, 9, 17300 Blanes, Spain

[5] Royal Botanic Gardens, Kew, Kew Green, Richmond TW9 3AE, UK

[6] Department of Computational Mathematics, Science & Engineering, Michigan State University, East Lansing, MI, USA

Authors for correspondence:

Daniel H. Chitwood

Email: dhchitwood@gmail.com

Manica Balant

Email: manica.balant@ibb.csic.es

Summary

- The iconic, palmately compound leaves of *Cannabis* have attracted significant attention in the past. However, investigations into the genetic basis of leaf shape or its connections to phytochemical composition have yielded inconclusive results. This is partly due to prominent changes in leaflet number within a single plant during development, which has so far prevented the proper use of common morphometric techniques.
- Here we present a new method that overcomes the challenge of nonhomologous landmarks in palmate, pinnate and lobed leaves, using *Cannabis* as an example. We

model corresponding pseudo-landmarks for each leaflet as angle-radius coordinates and model them as a function of leaflet to create continuous polynomial models, bypassing the problems associated with variable number of leaflets between leaves.

- We analyze 341 leaves from 24 individuals from nine *Cannabis* accessions. Using 3,591 pseudo-landmarks in modeled leaves, we accurately predict accession identity, leaflet number, and relative node number.
- Intra-leaf modeling offers a rapid, cost-effective means of identifying *Cannabis* accessions, making it a valuable tool for future taxonomic studies, cultivar recognition, and possibly chemical content analysis and sex identification, in addition to permitting the morphometric analysis of leaves in any species with variable numbers of leaflets or lobes.

Key words: *Cannabis*, development, geometric morphometrics, intra-leaf modeling, leaf morphology, leaf shape

INTRODUCTION

Cannabis sativa L. (hereafter referred to as *Cannabis*) is a versatile crop plant used by humans for a variety of purposes throughout history. Although today it is commonly associated with its psychoactive properties, traditional medicine has relied heavily on *Cannabis,* and it is also a valuable source of food and fibers (Clarke & Merlin, 2013). Genetic and archaeological evidence suggests that *Cannabis* was domesticated around 12,000 years ago in East Asia, initially serving as a multipurpose crop before separate selections for fiber and drug production emerged around 4,000 years ago (Ren *et al.*, 2021). Since then, widespread cultivation has facilitated its global distribution. Throughout the 20th century, *Cannabis* use was largely abandoned due to its illegal status in many parts of the world. However, recent legalization for recreational and/or medicinal purposes in many countries worldwide has led to a surge in the cannabis industry (*The Global Cannabis Report, 3rd Edition*, 2022).

Extensive *Cannabis* use has resulted in the development of numerous cultivars and strains that are well-suited to diverse uses and climates (Small, 2015). This significant

morphological and phytochemical diversity within the *Cannabis* genus poses challenges for taxonomic classification. Over the past two centuries, various taxonomic approaches based on genetics, morphology, and phytochemistry have been proposed (McPartland & Small, 2020). Some scientists advocated for a polytypic classification, recognizing the presence of two (Lamarck & Poiret, 1783; Zhukovskii, 1971; Hillig, 2005a) or three (Emboden, 1974; Schultes *et al.*, 1974; Hillig, 2005b; Clarke & Merlin, 2013) species with multiple subspecies, while others argued for a monotypic genus, considering only a single species, *Cannabis sativa* (Small & Cronquist, 1976; Sawler *et al.*, 2015; Small, 2015; McPartland, 2018; McPartland & Small, 2020; Ren *et al.*, 2021). Hillig (2005a) introduced a classification system based on biotypes, considering molecular, morphological, and phytochemical data. He proposed dividing *Cannabis* into two species, *C. sativa* and *C. indica* Lam., and six biotypes: *C. indica* as narrow-leaflet drug (NLD), wide-leaflet drug (WLD), hemp and feral biotype, and *C. sativa* as hemp and feral biotype. Recently, Lapierre *et al.* (2023) conducted a comprehensive taxonomic review of the *Cannabis* genus and based on available genetic data, strongly supported the theory that *Cannabis* is a highly diverse monotypic species.

Apart from taxonomic classification, *Cannabis* is often categorized based on its cultivation purpose, morphology, and chemical composition. Fiber-type plants, commonly known as hemp, are primarily grown for fiber and seed production. These plants contain less than 0.3% of the psychoactive compound THC (Δ9-tetrahydrocannabinol), while drug-type plants, often referred to as marijuana and medicinal cannabis, can contain higher levels of THC (Hurgobin *et al.*, 2021). *Cannabis* plants can also be separated based on the ratio of two major cannabinoids THC and CBD (cannabidiol) into Type I (THC dominant), Type II (balanced CBD/THC ratio), and Type III plants (CBD dominant) (Small & Beckstead, 1973). In the medicinal and recreational cannabis industries plants are normally categorized as ‘sativa’, ‘indica’, or ‘hybrid’. Taller plants with narrow leaflets and high THC percentage are called ‘sativa’, while shorter and bushier plants with wider leaflets and high percentages of both CBD and THC are called ‘indica’. Plants with intermediate characters are called ‘hybrids’ (McPartland & Guy, 2017). While the classification of *Cannabis* into ‘indica’ and ‘sativa’ is not supported by genetic data, the visible differences in leaflet width have long been a significant characteristic used to visually discriminate different types of *Cannabis*.

96 *Cannabis* arguably possesses one of the most iconic leaves among all plants. Its palmately
97 compound leaves with a varying number of leaflets are a popular culture symbol. *Cannabis*
98 exhibits a remarkable degree of phenotypic plasticity, further accentuated by selection
99 pressure during the domestication process (Small, 2015). Extensive variability in leaf
100 morphology has already been described by Quimby *et al.* (1973) and later Anderson (1980),
101 who was the first to quantify the width, length, and ratio of the central leaflet. This or
102 similar methods were then commonly used in studies investigating the morphological
103 characteristics of *Cannabis* species, subspecies, cultivars, biotypes and chemotypes (Small *et*
104 *al.*, 1976; de Meijer *et al.*, 1992; de Meijer & Keizer, 1996; Hillig, 2005a; Clarke & Merlin,
105 2013; Lynch *et al.*, 2016; Karlov *et al.*, 2017; Parsons *et al.*, 2019; McPartland & Small, 2020;
106 Carlson *et al.*, 2021; Islam *et al.*, 2021; Jin *et al.*, 2021a; Vergara *et al.*, 2021; Buzna & Sala,
107 2022; Chen *et al.*, 2022; Murovec *et al.*, 2022), often with contradictory results. Leaf shape
108 has therefore played an important and sometimes controversial role in *Cannabis* taxonomy.
109 While researchers in previous *Cannabis* studies were aware of enormous plasticity and the
110 effect the environment has on leaf shape (Vergara *et al.*, 2021; Murovec *et al.*, 2022), they
111 very rarely paid attention to the effects of developmental processes, even though
112 heteroblastic changes (differences in leaf shape arising from juvenile-to-adult phase
113 transitions in the meristem) profoundly affect the arrangement and shape of *Cannabis*
114 leaves along the shoot. While some studies briefly mention the developmental changes of
115 leaves (Hillig, 2005a; Carlson *et al.*, 2021; Jin *et al.*, 2021b; Spitzer-Rimon *et al.*, 2022), the
116 only two studies focusing on heteroblastic phase changes in leaves along the plant axis were
117 done by Heslop-Harrison and Heslop-Harrison (1958) and Hesami *et al*. (2023). In the lower
118 part of the shoot *Cannabis* leaves exhibit opposite phyllotaxy and one to three leaflets,
119 transitioning to alternate phyllotaxy and leaves with up to 11 or 13 leaflets in the upper
120 section (Hillig, 2005a; Clarke & Merlin, 2013; Small, 2015). Additionally, the changes in
121 leaflet number are not uniform between different *Cannabis* accessions (Hillig, 2005a). These
122 changes during development not only complicate categorization of plant accessions based
123 on leaf shape, but also prevent the use of morphometric techniques.
124
125 Morphometrics is the quantitative analysis of shape. It includes a wide range of methods,
126 from measuring allometric differences in dimensions like lengths, widths, and angles in
127 relation to size (Niklas, 1994), to geometric techniques that measure shape

comprehensively, like elliptical Fourier (EFDs; Kuhl & Giardina, 1982) and landmark-based analyses (Bookstein, 1997). It can be used to classify species and to separate effects on shape arising from genetic, developmental, and environmental mechanisms (Chitwood & Sinha, 2016). Historically the field of ampelography (ἄμπελος, 'vine' + γράφος, 'writing'; Ravaz, 1902; Galet, 1952; Galet & trans. Morton, 1979) relied heavily on leaf shape to distinguish grapevine varieties. Unlike *Cannabis,* grapevine leaves have a consistent number of lobes, sinuses, and other associated homologous points that can be used for both landmark-based and EFD morphometric analysis (Chitwood *et al.*, 2014; Chitwood, 2021) to disentangle genetic (Demmings *et al.*, 2019), developmental (Chitwood *et al.*, 2016a; Bryson *et al.*, 2020; Migicovsky *et al.*, 2022), and environmental effects (Chitwood *et al.*, 2016b, 2021) embedded in leaf shapes.

The variable number of leaflets in *Cannabis* (and several other species with lobed, pinnate and palmate compound leaves) precludes analysis methods that rely on homologous, comparable points to measure shape comprehensively. Methods to automatically isolate individual leaflets (Failmezger *et al.*, 2018) or to model developmental trajectories, such as heteroblastic series (Biot *et al.*, 2016) were proposed previously for morphometrical analysis in such cases. In *Cannabis,* Vergara *et al.* (2021) used a landmark-based approach but were limited to analyzing the central and two most distal leaflets on each side, features that all *Cannabis* leaves except single-leaflet leaves possess, but which excludes most of the shape variation within a leaf.

Here, we seek to build on these works and conceptually extend our framework of continuously modeling leaflets within a palmate leaf. We model corresponding pseudo-landmarks for each leaflet as angle-radius coordinates relative to the petiolar junction and model angle and radius as a function of leaflet number to create continuous polynomial models that bypass the problems associated with variable numbers of leaflets between leaves. This enabled us to compare leaves with different numbers of leaflets within a plant and to discern differences between genotypes rather than the heteroblastic series. Analyzing over 300 *Cannabis* leaves, we model theoretical leaves with nine leaflets and 3,591 comparable pseudo-landmarks. Linear discriminant analysis (LDA) predicts accession, leaflet number, and relative node number with high accuracy. Intra-leaf modeling allows the application of morphometric techniques to comprehensively measure leaf shape in

160 *Cannabis*, enabling future taxonomic and developmental studies, cultivar recognition, and
161 possibly chemical content analysis and sex identification, in addition to permitting the
162 morphometric analysis of leaves in any species with variable numbers of leaflets or lobes.
163
164 **MATERIAL AND METHODS**
165
166 **Plant material and growing conditions**
167 This study includes 24 individuals from nine accessions of *Cannabis sativa* L. (Table **1**; Fig. **1**),
168 encompassing both wild/feral accessions and cultivated varieties with a wide distribution
169 area. The plants were grown from seeds in a growth chamber (Fitoclima D1200PLL, Aralab,
170 Portugal) to minimize the influence of the environment. Before sowing, the seeds were
171 sterilized overnight in a 5% H_2O_2 solution with the addition of Inex-A solution (Cosmocel,
172 Spain) at room temperature. Sterilized seeds were then transferred to Petri dishes and
173 placed in the growth chamber for germination. Once the first leaves emerged, the seedlings
174 were transferred to small peat pots with a pre-fertilized soil substrate (Kilomix Atami,
175 Spain). During this phase, the environmental conditions were set to 25°C, with an 18-hour
176 day and 6-hour night photoperiod, and a light intensity of 50 µmol $m^{-2}s^{-1}$ (Philips Master PL-
177 L 55W, Spain). After two weeks the surviving plants were transplanted to 3.5 l pots with the
178 same soil substrate. The light intensity was gradually increased to 300 µmol $m^{-2}s^{-1}$ over the
179 following week, without changing the photoperiod and temperature. The onset of flowering
180 in some *Cannabis* accessions is photoperiod dependent, therefore after four weeks, the
181 photoperiod was changed to 12 hours of daylight and 12 hours of darkness, and the light
182 intensity was gradually increased to 700 µmol $m^{-2}s^{-1}$ over the following week, while keeping
183 the temperature at 25°C. The plants remained in these environmental conditions until the
184 flowering stage. Plants received daily irrigation with tap water, without any application of
185 nutrient or phytosanitary control.
186
187

188 **Table 1** Accession details and number of leaves collected and analyzed in the study.

Accession ID	Accession type	Location/Cultivar name	Number of individuals	Number of leaves collected	Number of leaves analyzed
AM15	Wild/feral	Armenia, Sjunik marz, Goris town	5	90	74
BNG	Wild/feral	Bangladesh, Rangpur, Carmichael College Campus	1	14	10
FUT75	Cultivar	Futura 75	2	45	30
HU1	Wild/feral	Hungary, Nyírvasvári	4	83	68
IK	Landrace	India, Kerala	4	92	53
IKL	Landrace	India, Kullu	4	69	47
MAR	Landrace	Morocco, North Morocco	1	18	15
MN9	Wild/feral	Mongolia, Selenge aimag, Baruunburen sum	1	14	10
RO1	Wild/feral	Romania, Mangalija	2	36	34

189

190 **Leaf sampling and imaging**

191 A total of 461 leaves were sampled during the flowering stage, with the exception of
192 individuals from the accession IK, which did not begin to flower during the two-month
193 cultivation period. Leaves along the main axis of the plants were collected and immediately
194 scanned using a flatbed photograph scanner (Epson Perfection V370, Japan) at 1200 dpi
195 resolution. A piece of velvet fabric was placed between the leaf and the scanner cover to
196 avoid any shadows. No adjustments to the angle of individual leaflets were made before
197 scanning. Each leaf was scanned with a scale and a label indicating the node it originated
198 from, followed by a sequential lowercase letter, since typically two leaves are present per
199 node. Starting at the base of the plant, the first two leaves were labeled as leaves "a" and
200 "b" from node number 1, and so on, until the shoot apex.

201 *Cannabis* leaves display a marked heteroblastic, or juvenile-to-adult, leaf shape progression.
202 Mature, juvenile leaves located on the first node at the base of the plant usually have a
203 simple, serrated leaf. As node number increases so does the leaflet number, reaching a
204 maximum of 9 to 13 leaflets in young, adult leaves at the growing tip. Eventually leaves
205 transition into an inflorescence type. During this transition, the number of leaflets per leaf
206 starts to decrease again until the top of the inflorescence. Leaves at the shoot base have
207 opposite phyllotaxy and transition to alternate phyllotaxy in the upper section on the stem
208 and inflorescence (Heslop-Harrison & Heslop-Harrison, 1958; Hillig, 2004; Potter, 2009;

209 Spitzer-Rimon *et al.*, 2022). To ensure that only stem leaves were included in our analysis,
210 we separated the two types (i.e., stem and inflorescence leaves) based on the point where
211 the decrease in the number of leaflets appeared. This point determined the “total node
212 number”, the number of nodes per plant used for further analysis. Total node number
213 varied among individuals. To compare node positions, a relative node number was
214 calculated, which was defined by the node position divided by the total node number for
215 the individual plant, where zero is at the plant base and one at the last node included in the
216 analysis (Fig. **1**). Because of the nature of plant growth, the leaves at the base of the plant
217 were frequently too senesced to be incorporated in the analysis or were entirely lost.
218 Nevertheless, the nodes could still be identified, which allowed them to be taken into
219 account in the calculation of relative node number.

220 **Image analysis and landmarking**

221 After eliminating damaged and deformed leaves (39), simple leaves (4), leaves with even
222 leaflet numbers (3) and leaves with relative node values above one (57), a total of 358
223 *Cannabis* leaves were used for image analysis and landmarking. Photoshop was used to
224 separate petioles and leaflets smaller than 1 cm from the rest of the leaf. The leaf outlines
225 were then extracted and saved using Python modules NumPy (Harris *et al.*, 2020),
226 Matplotlib (Hunter, 2007) and OpenCV (Bradski, 2000). The code for extracting and plotting
227 the leaf outlines can be found on GitHub
228 (https://github.com/BalantM/Cannabis_leaf_morpho_updated). The *x* and *y* coordinates of
229 blade outlines and landmarks were extracted using ImageJ (Abràmoff *et al.*, 2004). The
230 outline was extracted using the *wand* tool (setting tolerance to 20 and including "smooth if
231 thresholded" option) and the landmarks were placed using the *multi-point* tool.

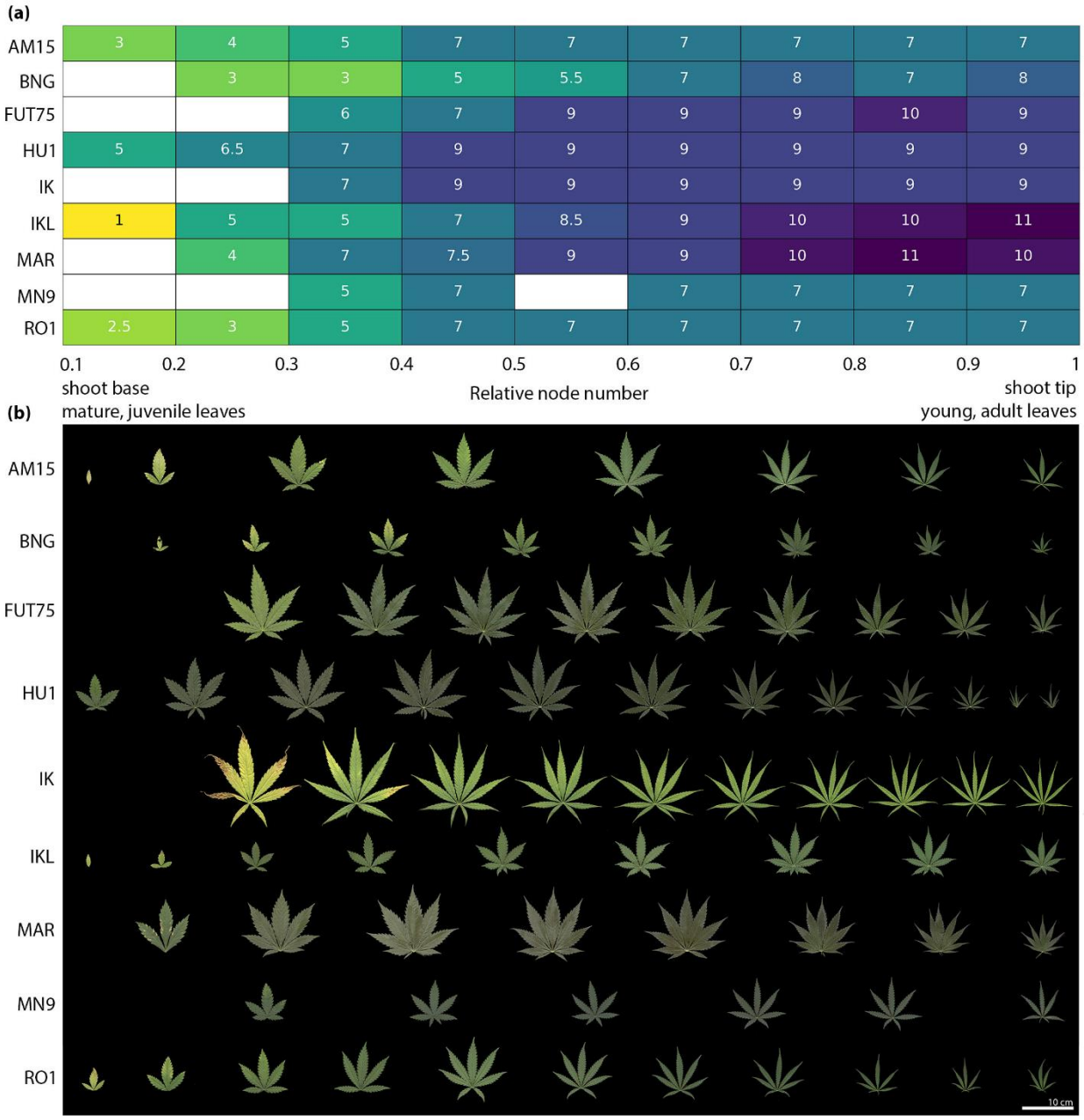

Fig. 1 Changes in the leaf shape and leaflet number during the development in nine *Cannabis* accessions. (a) Median values for all available leaflet number for each relative node number for the nine *Cannabis* accessions. (b) Changes in leaf shape between different developmental stages in different *Cannabis* accessions.

Initially, landmarks were placed at the beginning and end of each leaflet, starting from the lower left side, and continuing to the lower right side of the leaf outline. Subsequently, landmarks were placed in the same order on the tips of the leaflets. The final landmark was positioned at the center of the petiolar junction (Fig. **2**, second column). These landmarks delimit the boundaries of the leaflets so that equidistant pseudo-landmarks can later be

placed along the contour. The number of landmarks per leaf ranged from 10 to 28, depending on the leaflet number. The raw data containing the coordinates for leaf outlines and landmarks can be accessed on GitHub (https://github.com/BalantM/Cannabis_leaf_morpho_updated).

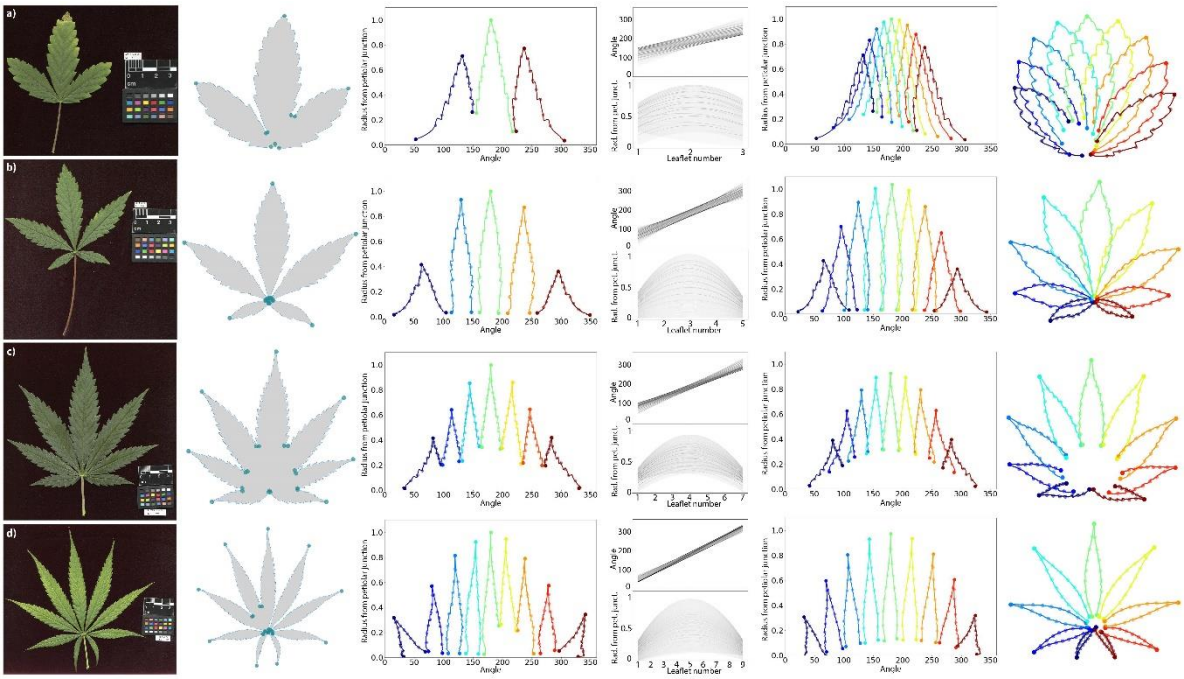

Fig. 2 The process of modeling theoretical leaves for a leaf with (a) three leaflets from accession AM15, (b) five leaflets from accession IKL, (c) seven leaflets from accession FUT75, and (d) nine leaflets from accession IK. The first column shows the scans of the leaves, which we use to extract the outline and place the landmarks on the tip, start, and end of each leaflet and on the petiolar junction (second column). These coordinates are used to generate 200 equidistant pseudo-landmarks on each side of each leaflet, sharing the landmark on the tip of the leaflet for a total of 399 pseudo-landmarks. These coordinates are then converted into polar coordinates. Each transformed leaflet is defined with 399 equidistant pseudo-landmarks, with three landmarks, two at the base and one at the tip. Large points are placed every 25 pseudo-landmarks to emphasize that leaflet outlines are defined by points (third column). Second degree polynomials for angles and for radius from petiolar junction are then fitted through these 399 pseudo-landmarks (fourth column). A modeled theoretical leaf with nine leaflets defined by 3,591 pseudo-landmarks can then be modeled using the collection of 798 polynomial models for each leaf (399 polynomial

261 models for angles and 399 for radius from petiolar junction) (fifth column) and visualized in
262 the cartesian coordinate system (sixth column).
263
264 **Reconstruction of the new modeled leaves**
265 To analyze leaves with different numbers of leaflets, pseudo-landmarks of each leaflet were
266 modeled as 2nd degree polynomial models of angles and radius as functions of leaflet
267 number within a leaf, in order to use the models to construct a modeled theoretical leaf
268 with a desired number of leaflets. The Python code, presented as a Jupyter notebook with
269 detailed description, is available on GitHub
270 (https://github.com/BalantM/Cannabis_leaf_morpho_updated). The *x* and *y* coordinates of
271 the leaf outline were first interpolated to create an arbitrarily high number of coordinates to
272 increase resolution of the leaf outline. The coordinates of manually selected landmarks
273 were then compared against the high-resolution coordinates of the leaf outline and the
274 nearest neighboring point of the high-resolution coordinates to each original landmark was
275 identified and specified as the new landmark point. Next, the outline and new landmark
276 coordinates were rotated, translated, and scaled so that the central leaflet had a length of
277 one and pointed in the same direction. The transformed points were then interpolated to
278 generate 200 pseudo-landmarks on each side of each leaflet (from the landmark at the
279 bottom until the tip of the leaflet), sharing the landmark on the tip of the leaflet (i.e., a total
280 of 399 pseudo-landmarks per leaflet). These pseudo-landmarks were then converted to
281 polar coordinates, where each point was defined by a radius and angle relative to the
282 landmark of the petiolar junction and tip of the central leaflet (Fig. **2**, third column).
283
284 Using the polar coordinates of each leaflet, 2nd degree polynomial models for *x* (angle) and *y*
285 (radius from petiolar junction) values were fit through each of the 399 corresponding
286 pseudo-landmarks for each leaflet using the Python *scipy.optimize.curve_fit* function
287 (Virtanen *et al.*, 2020), modeling angle and radius as a function of leaflet number (Fig. **2**,
288 fourth column). Using the coefficients for 2nd degree polynomial models, we then model
289 each pseudo-landmark as a function of leaflet number to reconstruct the new theoretical
290 leaf with an arbitrary number of leaflets. Meaning that for each leaflet, each of the 399 *x*
291 and *y* pseudo-landmarks (i.e., angle and radius from petiolar junction coordinates) was
292 calculated using the 2nd degree polynomial function, with coefficients obtained from the

previous step, and the newly defined leaflet number (9 in this case). The optimal number of reconstructed leaflets was tested for the best prediction accuracy in Linear discriminant analysis modeling and the highest accuracy was achieved by reconstructing 9 leaflets (Table **S1**). It is important to note that the reconstructions start with the first real leaflet and end with the last real leaflet. These 9 reconstructed leaflets are then equally divided between these two points.

Nine leaflets were reconstructed using the collection of coefficients of 789 2nd degree polynomial models for each leaf; the 399 models for angle were used to model theoretical *x* (i.e., angle) and 399 models for radius were used to model theoretical *y* (i.e., radius from petiolar junction) pseudo-landmarks as a function of nine leaflets.

The coordinates defining the 3,591 pseudo-landmarks for each of the modeled leaves (399 pseudo-landmarks for each of the 9 reconstructed leaflets) were then plotted and visually inspected. We detected 17 inaccurately modeled leaves, most likely caused by the position of the petiole landmark compared to the landmark marking the start and end landmarks of the leaflet. A total of 341 *Cannabis* leaves were then used in the analysis.

Validation of the leaf modeling approach

To validate our modeling approach, we extracted the polar coordinates of the original central leaflets (Fig. **3a**) and central leaflets of the modeled leaves (Fig. **3b**) and used them in Procrustes analysis using *Procrustes* function from scipy.spatial module (Virtanen *et al.*, 2020). Procrustes analysis minimizes the distance between all points for a set of landmarks/pseudo-landmarks between two samples through translation, rotation, and scaling, and returns new points of the two sets, superimposed to each other (Fig. **3c**). We then calculated the Procrustes distance between the original central leaflet (angle and radius coordinates) to its corresponding modeled reconstruction, a measure of their similarity. The mean distance was calculated and compared to that of simulated bootstrapped mean values by resampling (10,000 resamples) through randomly sorting original leaflet coordinates against coordinates of reconstructed leaflets.

323 **Morphometric analysis of the central leaflet shape using previously established**
324 **methodologies**
325 The width-to-length ratio (W/L ratio), first described by Anderson (1980), was frequently
326 used to describe the shape of *Cannabis* leaves or even differentiate between different
327 *Cannabis* taxa. With previously established morphometric methods, the shape analysis of
328 central leaflets (that all leaves share) would also be possible, using EFDs or pseudo-
329 landmarks approach. To evaluate the effectiveness of these two previous methods for the
330 shape analysis of *Cannabis* leaves, we first extracted the Cartesian coordinates of central
331 leaflets (Fig. **4a**), that were previously scaled, rotated and translated, so that they were all
332 pointing in the same direction and had the length of one. We then interpolated 200 pseudo-
333 landmarks on each side of each leaflet, sharing the landmark on the tip of the leaflet (i.e., a
334 total of 399 pseudo-landmarks per leaflet).
335 To measure the W/L ratio, we calculated width of the leaf (as the leaves were already
336 normalized to length of one), calculating the minimum bounding rectangle. The distribution
337 of widths was then plotted using Python package *seaborn.kdeplot*. To see if the analyzed
338 accessions differed significantly in their W/L ratios, Kruskal-Wallis test was calculated using
339 *stats.kruskal* function from the scipy.stats module. To see which of the accessions differ in
340 W/L ratio, we calculated Dunn's Multiple Comparison Test with *scikit_posthocs* package in
341 Python (Terpilowski, 2019), using the *posthoc_dunn* function.
342
343 Linear discriminant analysis (LDA) was applied to model accession, leaflet number, and
344 relative node number as the function of central leaflet coordinate values, using the
345 *LinearDiscriminantAnalysis* function from the scikit-learn module in Python (Pedregosa *et*
346 *al.*, 2011). To test the performance of the LDA model, the dataset was divided into two
347 parts. Since most of the analyzed leaves exhibit opposite phyllotaxy, wherein the nodes
348 were represented by two leaves (a and b) in the same developmental phase with the same
349 number of leaflets, the dataset was split into a training dataset (leaf a) comprising 180
350 leaves and a test dataset (leaf b) containing 161 leaves. The *predict* function from
351 *LinearDiscriminantAnalysis* in the scikit-learn module was used to predict the accession
352 identity, leaflet number, and relative node number, based on the central leaflet coordinate
353 values. The accuracy of the LDA model was calculated and visualized using the function
354 *confusion_matrix* from scikit-learn. Spearman Rank Correlation was calculated for true and

predicted results for relative node number with *spearmanr* function from the scipy.stats module.

Data analysis of modeled leaves

A principal component analysis (PCA) was performed on the coordinates of the modeled leaves using scikit-learn module in Python and proportions of explained variance for each principal component and the cumulative variance was calculated. Points representing the leaves were colored by the accession identity, leaflet number, or relative node number (Fig. **5**). To see which of the first two PCs explains most of the leaf shape variation for accessions, leaflet number and relative node number, Kruskal-Wallis test was calculated using *stats.kruskal* function from the scipy.stats module. To visualize an average leaf for each accession, leaflet number, and relative node number, the average coordinate values of modeled leaves were calculated for each of the categories and plotted using the Matplotlib module in Python (Fig. **5**).

To see if the modeled leaves can be used to model accession, leaflet number, and relative node number, we followed the same steps as before for shape analysis of central leaflet. Linear discriminant analysis (LDA) was applied to model accession, leaflet number, and relative node number. The dataset was again split into a training and test dataset to see if we were able to predict accession, leaflet number, and relative node number identity, based on the coordinates of modeled leaves. The same was done on a combined dataset with 3990 coordinates, created by concatenating coordinates of modeled leaves and the coordinates of the original central leaflets.

RESULTS

Heteroblastic changes in leaflet number along the main axis

Over 460 *Cannabis sativa* leaves were collected, scanned, and their leaflet number recorded. The leaves exhibited a profound heteroblastic juvenile-to-adult progression along the axis, but the changes were not uniform between the accessions (Fig. **1**). In the few rare cases where the leaves in the lower nodes were present, the first nodes always started with a simple serrated leaf. The second leaf usually had three leaflets and the most frequent

leaflet number in the third node was five. However, the leaflet number in the nodes above varied dramatically between accessions. The number of nodes before the transition into the inflorescence in each of the plants also varied. We therefore calculated relative node number, a fractional number between 0 at the shoot base to 1 at the inflorescence transition, to compare the node leaves between plants.

Validation of the leaf modeling approach

The modeling approach was validated by calculating the mean Procrustes distance of modeled central leaflet coordinates to original central leaflet coordinates using 10,000 bootstrap replicas, assessing resampled means against the actual Procrustes mean value. None of the 10,000 resamples yielded a mean lower than the observed Procrustes value, confirming the robustness of the novel modeling approach (Fig. **3d**).

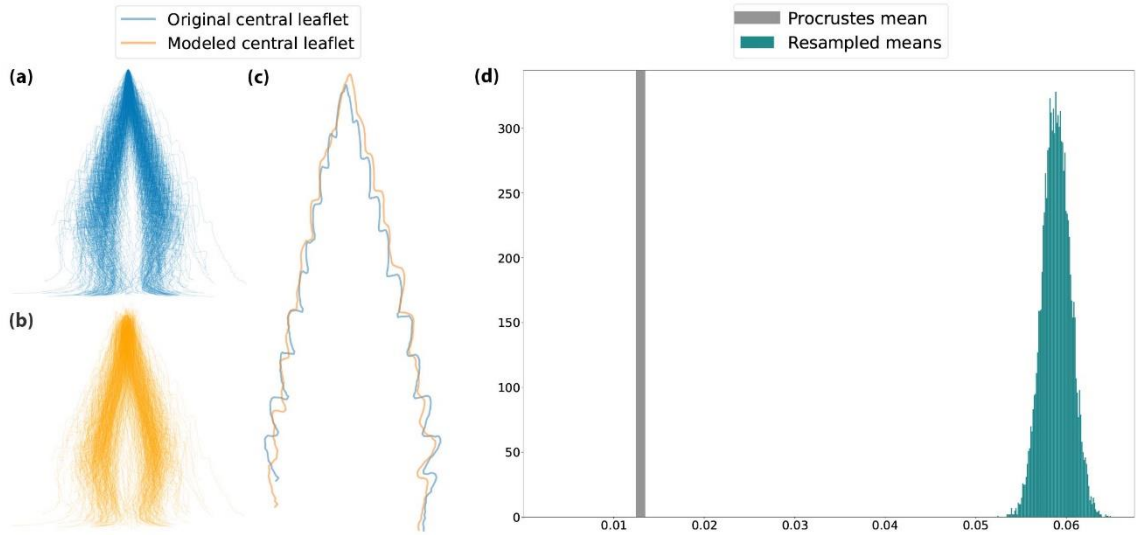

Fig. 3 Modeling approach validation using Procrustes analysis and bootstrap resampling. The (a) original and (b) modeled central leaflets in polar coordinate system were superimposed (c) and Procrustes distances calculated. (d) The resampled mean was plotted as a distribution (green histogram) against the actual Procrustes mean (grey vertical line).

Width-to-length (W/L) ratio and central leaflet shape analysis

Our results indicate that the width-to-length (W/L) ratio of central leaflets is not able to differentiate well between different *Cannabis* leaf accessions based on this information

alone (Fig. **4**). While the Kruskal-Wallis test did show overall significance between accessions (Table **S2**), Dunn's post hoc indicated significance in leaf morphology for just one accession (Table **S3**). The W/L ratio significantly differs from the rest only for the IK accession, characterized by particularly narrow leaves (Table **S3**). The Kruskal-Wallis test was also significant for leaflet numbers and relative node numbers (Table **S2**). Dunn's post hoc revealed that while we can differentiate between leaflet numbers based on the W/L ratio of central leaflet, we can only separate the lower and higher relative nodes (Table **S3**).

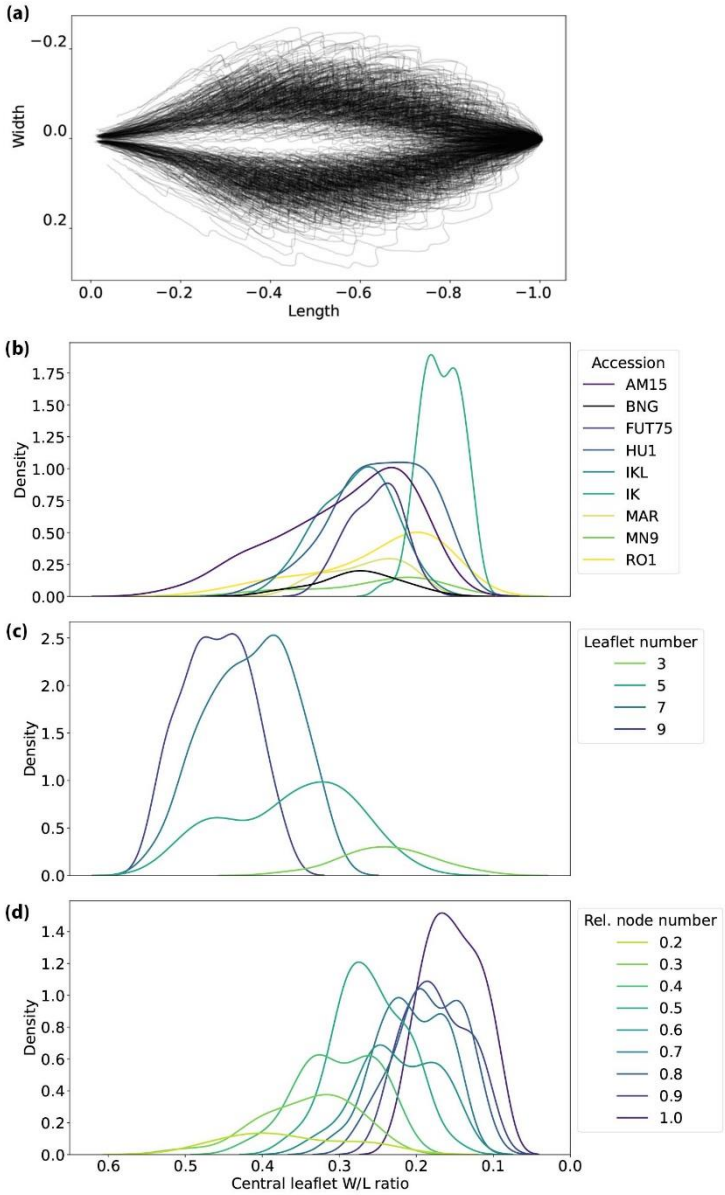

Fig. 4 Analysis of leaf shape using the approach adapted from Anderson (1980). (a) Visualization of the 341 central leaflets used in the analysis. W/L ratios plotted by (b) accession, (c) leaflet number and (d) relative node number.

To test whether the outline of the central leaflet can better predict the genetic and developmental identity of *Cannabis* leaves, we used Linear discriminant analysis (LDA) to

439 model each factor as a function of 399 pseudo-landmark points defining the shape of
440 central leaflet (Fig. **5a-c**). To evaluate model accuracy, accession was treated as a categorical
441 variable, as was leaflet number, as it not only has a small number of levels (3, 5, 7, and 9
442 leaflets), but each level is well separated from the others. To evaluate the accuracy of
443 relative node number, we treated it as a continuous variable, due to a high number of levels
444 (9) that continuously overlap with each other. Models revealed low accuracy, as the
445 accession was correctly determined only in 47.20% (Table **2**). The LDA model for the shape
446 of central leaflet showed no overlap for the accessions IK and MN9, but the remaining
447 accessions showed significant overlap (Fig. **5a**). The confusion matrix revealed that only two
448 accessions were correctly identified more than half the time (AM15 – 53.13% and IK –
449 71.43% prediction accuracy) (Fig. **5d**). The LDA model showed better success when
450 identifying the leaflet number (57.76% overall accuracy) and relative node number, where
451 the true and predicted values show significant, but moderate correlation (rho = 0.629, $p <$
452 0.0001) (Fig**. 5b, c, e, f**; Table **2**).
453
454 **Table 2** Predictive power of genetic and developmental identities using the LDA model on
455 the central leaflet shape.

	Correct prediction [n]	**False prediction [n]**	**Prediction accuracy [%]**	**Correlation coefficient [rho]**	**p value**
Accession	76	85	47.20	NA	NA
Leaflet number	93	68	57.76	NA	NA
Relative node number	NA	NA	NA	0.629	< 0.0001

456

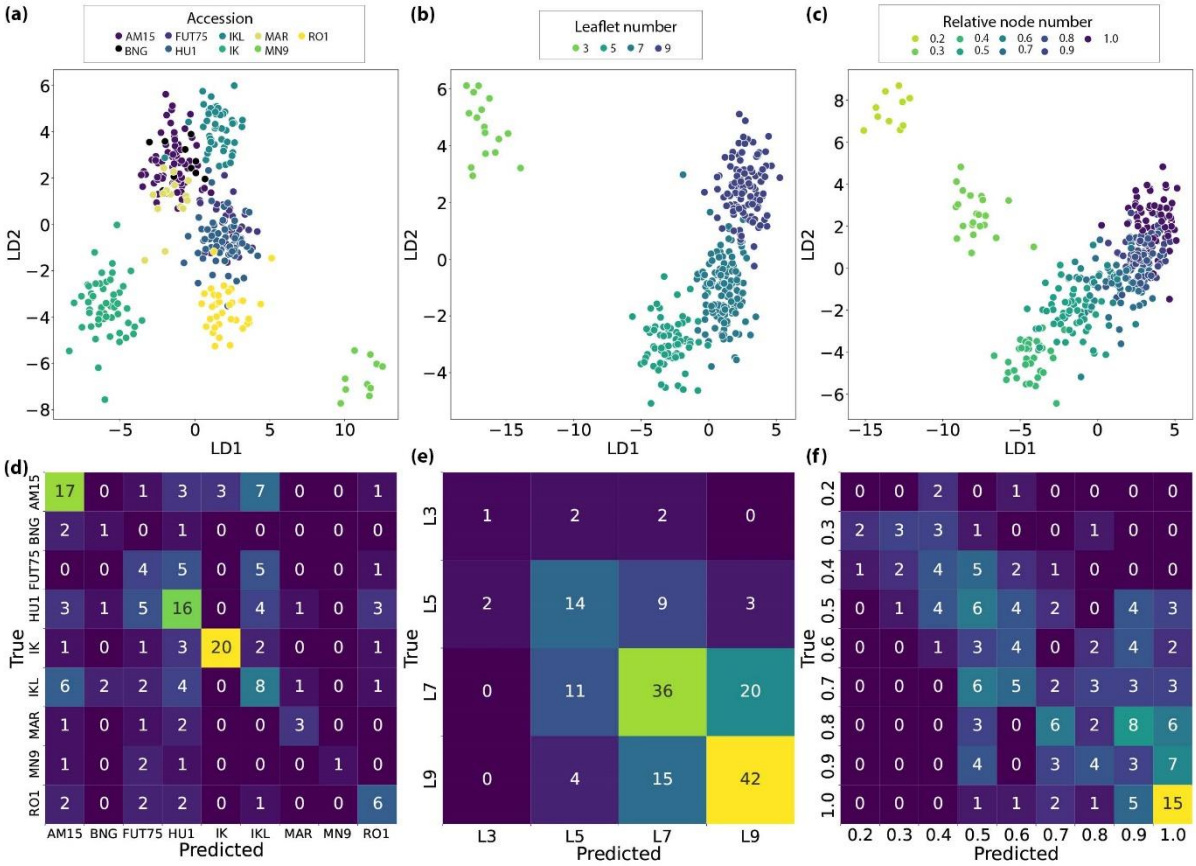

Fig. 5 Accession, leaflet number and relative node numbers prediction of *Cannabis* leaves using the outline of central leaflets. Linear discriminant analysis (LDA) plots for (a) accession, (b) leaflet number and (c) relative node number. In the lower row, the confusion matrices show the true and predicted identities for (d) accessions, (e) leaflet number, and (f) relative node number using the LDA model on the split test and train dataset.

Principal component analysis on modeled leaves (PCA)

Using the outline and landmark coordinates of 341 leaves, we modeled new theoretical leaves, all with nine leaflets. Each leaf is defined by 3,591 pseudo-landmarks, which overcomes the problems associated with variable leaflet numbers and permits dimension reduction using PCA (Fig. **6a-c**) and the visualization of average *Cannabis* leaves (Fig. **6d-f**). The first and second PCs account for 85.85% and 7.25% of the shape variation, respectively (Fig. **6a-c**). Examining the PC1 and PC2 with Kruskal-Wallis test reveals that that accession, leaflet number and relative node number all vary significantly along the first PC axis. The variation along the PC2 for accession and leaflet number is less pronounced, however still significant, while PC2 values for relative node numbers do not vary significantly (Fig. **6**; Table

474 **3**). This indicates that the changes in leaf shape between accessions are not independent
475 from developmental variation. That a facet of variation in accession leaf shape covaries with
476 developmental variation across the shoot in leaflet and relative node number suggests a
477 heterochronic mechanism by which accession differences in leaf shape arise from changes
478 in developmental timing, and contrasts with the historical focus on changes in timing arising
479 from plasticity (Goebel, 1908; Ashby, 1948).
480
481 **Table 3** Kruskal-Wallis test was used to test the leaf shape variation along PC1 and PC2 for
482 accessions, leaflet number and relative node number.

	PC1		**PC2**	
	H	**p value**	**H**	**p value**
Accession	112.64	**p < 0.0001**	18.57	**p < 0.05**
Leaflet number	204.36	**p < 0.0001**	10.75	**p < 0.05**
Relative node number	49.73	**p < 0.0001**	2.98	p > 0.05

483
484 The average modeled leaf shapes show that the most pronounced change in leaf shape
485 between the accessions and during the development corresponds to narrow vs. wide
486 leaflets that are stereotypical descriptions of *sativa* vs. *indica* or *wide*- vs. *narrow- leaflet*
487 drug varieties. Furthermore, the leaves with the lower number of leaflets have more acute
488 leaflet tips, that slowly transition into acuminate. Additionally, the outer leaflets in the
489 leaves from lower nodes (and in certain accessions) are longer, compared to the central
490 leaflet, and become shorter higher up (Fig. **6d-e**).
491

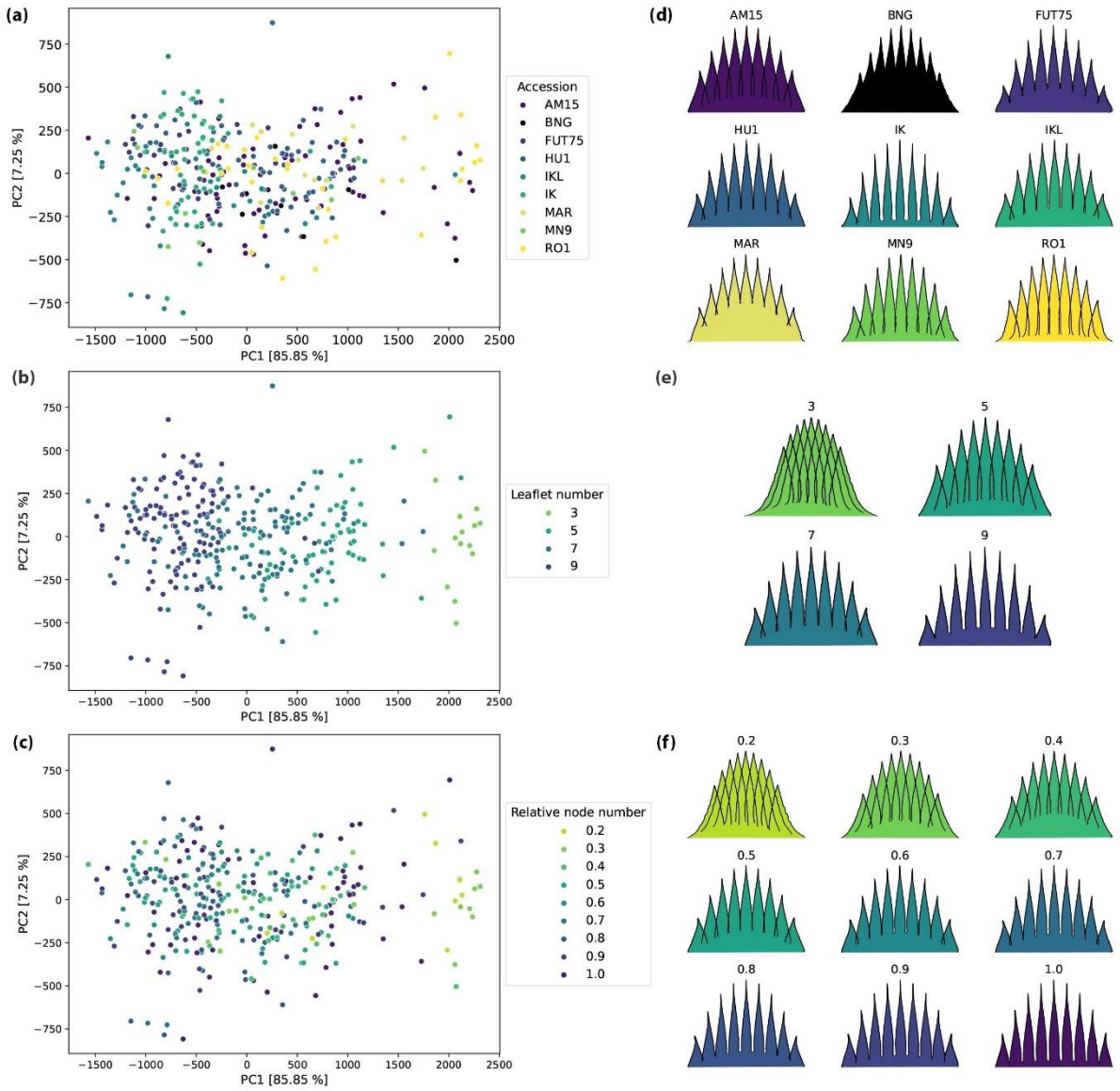

Fig. 6 Principal component analysis (PCA) of the accessions performed on modeled leaves using the 3,591 pseudo-landmarks (a-c). The first PC explains 85.58% and the second 7.25% of variation. The images on the right show the average modeled leaf shapes for each of the (d) nine analyzed accessions, (e) leaflet number and (f) relative node number.

LDA and prediction of genetic and developmental identities on modeled leaves

As in the analysis of central leaflet shape before, we used LDA to model accession, leaflet number and relative node number as a function of all 3,591 pseudo-landmark points defining the complete modeled leaves (Fig. **7**). Accuracy of the model was calculated on the split dataset, treating accession and leaflet number as categorical and relative node number as continuous variable. LDA models for both accession and leaflet number were highly

504 accurate (73.29% and 99.38%, respectively) (Table **4**), significantly improving the results
505 obtained by analyzing solely the outline of the central leaflet (Table **2)**. The model for
506 relative node number is highly accurate as well, as inferred by a highly significant
507 Spearman's rank correlation coefficient value between actual and predicted values (rho =
508 0.747, $p < 0.0001$) (Table **4**).
509
510 **Table 4** Predictive power of genetic and developmental identities using the LDA model on
511 the modeled leaves.

	Correct prediction [n]	False prediction [n]	Prediction accuracy [%]	Correlation coefficient [rho]	p value
Accession	118	43	73.29	NA	NA
Leaflet number	160	1	99.38	NA	NA
Relative node number	NA	NA	NA	0.747	< 0.0001

512
513 A confusion matrix reveals that the LDA model in most cases had a high accuracy for
514 predicting accession identity (Fig. **7d**; Table **4**), much higher, as compared to the accuracy
515 achieved by using only the outline of the central leaflet (Fig. **5d,** Table **2)**. Accessions IK, RO1,
516 and MN9 show practically no overlap in LDA space, while AM15, BNG, FUT75, HU1, IKL and
517 MAR show more overlap (Fig. **7a**). The model showed an almost 100% success rate in
518 determining leaflet number, again, much higher than before.
519 Results of both methods revealed that leaves with only 3 leaflets are markedly different
520 from the rest, and the prediction model on theoretical leaves consistently classified them
521 correctly (Fig. **7e**). Leaves with 5 to 9 leaflets showed less pronounced differences in shape,
522 resulting in a slightly lower accuracy of the prediction model for these cases. However, an
523 examination of the confusion matrix revealed that misclassifications only occurred once
524 between leaves with neighboring leaflet numbers (7 and 9 leaflets) (Fig. **7e**). The marked
525 difference in shape of leaves with 3 leaflets from the rest may suggest that this
526 developmental mechanism is biased towards variation at the base of the shoot. Similar to
527 leaflet number, the confusion matrix for the relative node model reveals high rates of
528 misclassification between the neighboring relative node numbers, as is expected, and leaves
529 from lower nodes were very rarely classified as those from higher nodes (Fig. **5f**). A

530 pronounced change in leaf shape occurs between the relative nodes 0.3 and 0.4, while the
531 shape changes in later relative nodes are more gradual (Fig. **7c**).
532

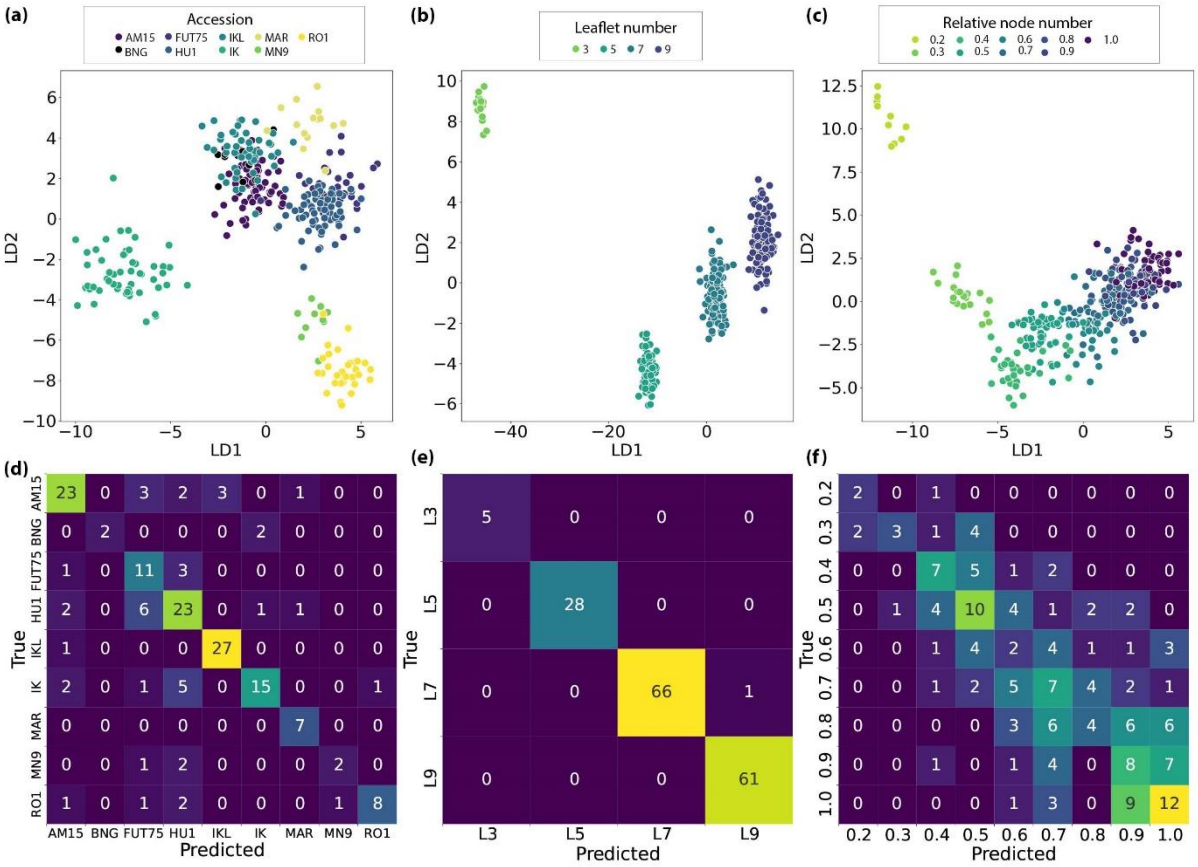

533

534 **Fig. 7** Accession, leaflet number and relative node numbers of *Cannabis* leaves can be
535 predicted independently of each other using modeled leaves. Linear discriminant analysis
536 (LDA) plots for (a) accession, (b) leaflet number and (c) relative node number. In the lower
537 row, the confusion matrices show the true and predicted identities for (d) accessions, (e)
538 leaflet number, and (f) relative node number using the LDA model on the split test and train
539 dataset.
540

541 Compared to only using the modeled leaves, the accuracy of the LDA model did not improve
542 significantly when using a combined dataset. A confusion matrix revealed that the LDA
543 model (Fig. **S1**) was slightly less successful in accession identity classification (71.43%) but
544 was higher for leaflet number (100%). The Spearman's rank correlation coefficient was
545 slightly higher and highly significant (rho = 0.748, $p < 0.0001$) (Table **5**).

546 **Table 5** Predictive power of genetic and developmental identities using the LDA model on a
547 combined dataset.

	Correct prediction [n]	False prediction [n]	Prediction accuracy [%]	Correlation coefficient [rho]	p value
Accession	115	46	71.43	NA	NA
Leaflet number	161	0	100	NA	NA
Relative node number	NA	NA	NA	0.787	< 0.0001

548

549 **DISCUSSION**

550

551 Like grapevines, striking variation in leaf shape (Fig. **1**) has historically played a significant
552 role in taxonomic classification of *Cannabis*. Leaf shape and differences in phyllotaxy were
553 among the characters Lamarck used to describe a new *Cannabis* species (Lamarck & Poiret,
554 1783). Anderson (1980) introduced a quantitative approach by quantifying the length-to-
555 width ratio of the central leaflet. Further studies using different characters—including plant
556 height, stem diameter, achene shape, and phytochemical profiles—to characterize
557 accessions have only confirmed the importance of leaf characteristics (Small *et al.*, 1976;
558 Hillig, 2005a). The central leaflet width-to-length ratio has been adopted by researchers as
559 one of the main characters for determining species, subspecies, biotypes and chemotypes of
560 *Cannabis* (Hillig, 2005a; Clarke & Merlin, 2013; McPartland & Small, 2020). However, this
561 method is only able to capture a limited aspect of leaf shape variation, neglecting other
562 important characteristics that we measure in this study, such as leaflet outlines, serrations,
563 angles, and relative changes in leaflet shape across the leaf. By modeling leaflet shape as a
564 function of leaflet number, we model theoretical leaves with the same number of leaflets
565 for which high densities of corresponding pseudo-landmarks capture high resolution shape
566 features (Fig. **2**). To validate the modeling approach, we have compared the outline of the
567 original central leaflet and the outline of the modeled theoretical central leaflet. The
568 Procrustes analysis showed that the two leaflets are very similar in shape, and that the
569 modeling is even able to preserve the serration pattern to some degree (Fig. **3c**). The
570 modeling approach validated using 10,000 bootstrap replicas confirmed the robustness of
571 the novel modeling approach (Fig. **3d**). This method can be applied not only on palmately
572 composed leaves as in *Cannabis* but is also possible to use on pinnate and lobed leaves. To

demonstrate the proof of concept, we applied the method to a pinnate leaf of *Cardamine flexuosa* With. and lobate leaf of *Quercus macrocarpa* Michx. (Fig. **8**), showing the method could be applied in other leaf types. However, the method needs to be improved before being applied to other species but shows the possible utility of intra-leaf modeling.

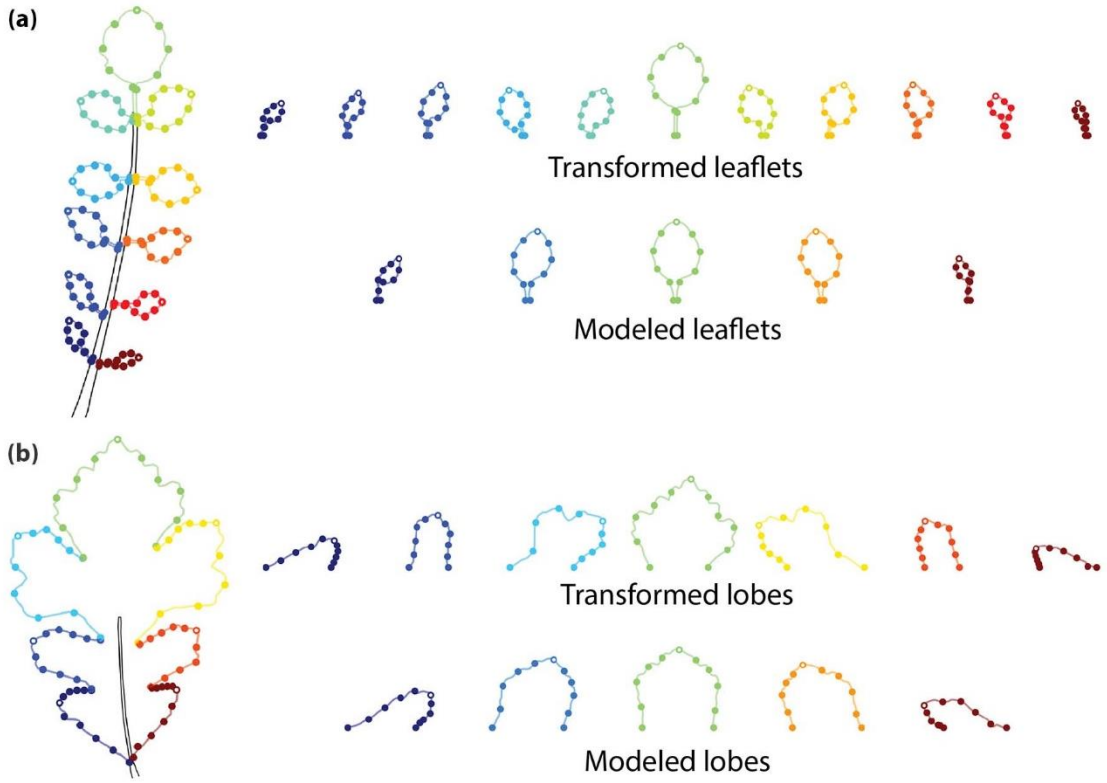

Fig. 8 Intra-leaf modeling of leaflets and lobes extended to pinnate leaves: Leaves from (a) *Cardamine flexuosa* and (b) *Quercus marcocarpa*. Leaflets and lobes are defined by 100 equidistant pseudo-landmarks on each side, each defined by three landmarks, two at the base and one at the tip. Large points are placed every 20 pseudo-landmarks to emphasize that leaflet outlines are defined by points. The landmarks defining the base of each leaflet or lobe are aligned to the rachis or midvein and the transformed leaflets and lobes have been oriented parallel to the rachis, as defined by the landmarks at their base. The modeled leaflets and lobes are created from 2nd degree polynomial models for each *x* and *y* coordinate value for each pseudo-landmark as a function of leaflet or lobe number. From these models, an equivalent number of modeled leaflets or lobes can be reconstructed (in this case, five), permitting morphometric analysis.

590 The method presented in this study can accurately determine accession based on leaf
591 shape, regardless of its developmental stage (Fig. **7a, d**). The method not only works
592 effectively on stabilized or cloned cultivar accessions but also on wild or feral accessions
593 cultivated from seed that can exhibit distinct plant phenotypes (Table **1**), indicating its
594 robustness and potential value in future germplasm classification. Compared to the low
595 accuracy and prediction ability of the previously known methods (W/L ratio and shape
596 analysis of central leaflets), the newly proposed method demonstrates significantly
597 improved results (Table **2, 4, S2, S3**). The combined dataset of both, data for modeled leaves
598 and outline of the central leaflet, did not return significantly better results, further
599 confirming the effectiveness of the new modelling approach.
600
601 When observing the shape changes between averaged leaves for accessions and between
602 developmental stages, the most obvious are changes in leaflet widths, similar to
603 stereotypical classifications of *sativa* and *indica* plants or *wide*- vs. *narrow- leaflet* drug
604 varieties. However, other important changes in shape occur, such as transition from acute
605 to acuminate leaflet tip and changes in the relative length of outer most leaflets compared
606 to the central leaflet, that previous methods could not successfully capture (Fig. **6d-f**). The
607 reliance on the non-quantitative leaf shape descriptors in previous methods has led to
608 numerous cultivars with unreliable names, inconsistent genetic origins, and phytochemical
609 profiles (Sawler *et al.*, 2015; Schwabe & McGlaughlin, 2019; Jin *et al.*, 2021a; Watts *et al.*,
610 2021). For example, Jin *et al.* (2021b) conducted a study on clones of 21 cultivars and found
611 a strong negative correlation between the width and length ratios of central leaflets and
612 CBD, and a positive correlation with THC; however, Vergara *et al.* (2021) and Murovec *et al.*
613 (2022) were unable to confirm these findings. All three studies used low-resolution
614 morphometric approaches. Sex of the plants also plays a crucial role in the cannabis
615 industry, where the presence of male plants and inevitable pollination leads to decreases in
616 cannabinoid production as plants shift the use of energy into seed development. Several
617 methods have been employed to differentiate between male and female plants at early
618 stages, but only genetic methods were successful so far (Toth *et al.*, 2020; Prentout *et al.*,
619 2020; Campbell *et al.*, 2021; Balant *et al.*, 2022; Torres *et al.*, 2022). Our results quantify the
620 variation in leaf shape between accessions that can potentially be used to classify accessions
621 and predict chemical profiles and plant sex faster and more accurately.

622

623 Unlike grapevine, where developmental variance is orthogonal and separate from genetic
624 variance, in *Cannabis* these two factors are correlated. That the developmental source of
625 variation is colinear with accession identity suggests that part of the differences between
626 accession leaf shape is explained by shifts in developmental timing, or heterochrony.
627 *Cannabis* plants demonstrate extreme phenotypic plasticity depending on the
628 environmental conditions in which they grows (Small, 2015). Some *Cannabis* accessions are
629 photoperiod dependent and can remain in vegetative phase for longer periods of time
630 under long-day conditions (typically 18h darkness and 6h light), until the transition to short-
631 day (12h of darkness and 12h of light) induces the formation of the apical inflorescence.
632 Previous investigations showed that other morphological changes, such as decrease in leaf
633 area, number of leaflets per leaf and serration number, occur after the change in the
634 environmental conditions one or two nodes after (Heslop-Harrison & Heslop-Harrison, 1958;
635 Hesami *et al.*, 2023). However, differences, especially in flowering time and growth rates
636 between cultivars have been observed before (de Meijer & Keizer, 1996; Hillig, 2005a;
637 Spitzer-Rimon *et al.*, 2019; Carlson *et al.*, 2021; Naim-Feil *et al.*, 2021; Stack *et al.*, 2021;
638 Chen *et al.*, 2022) and differences in cannabinoid profiles, leaflet index and phenological
639 development were proposed as characteristics to discriminate between them (de Meijer &
640 Keizer, 1996). Heterochronic shifts are apparent in the differential rates in which accessions
641 increase leaflet number across nodes, as well as maximum and average leaflet counts across
642 accessions (Fig. **1**). Remarkably, stages in developmental timing are conserved despite being
643 shifted. For example, a significant shape change exhibited between the leaves with 3 and
644 leaves with 5 leaflets, with leaflets becoming more acuminate and narrower. In contrast,
645 changes in shape between leaves with a higher number of leaflets were more gradual.
646 Additionally, we observed a similar shift in leaf shape between the nodes 0.3 and 0.4,
647 potentially indicating a transition between the juvenile and adult phases of leaf
648 development. Similar results were obtained in previous research. Spitzer-Rimon *et al.* (2022)
649 demonstrated that flowering buds were initiated at node 7, while Moliterni *et al.* (2004)
650 analyzing a different cultivar, found developing flower buds in the 4th node, suggesting that
651 transitions in growth phases are conserved but not synchronized across cultivars. Due to the
652 differences in developmental timing between accessions, the use of continuous models

along the shoot could further improve the success predicting accession identity, as was the case in grapevine (Bryson *et al.*, 2020).

Conclusions

In grapevine, leaf shape has long been utilized for variety identification. However, in the case of *Cannabis*, previous attempts were hindered by the variability in leaflet numbers. In this study, we present a pioneering method that successfully addresses this issue. By generating theoretical leaves with customizable leaflet counts, we can now employ high-resolution morphometric techniques to accurately classify different wild/feral and cultivated *Cannabis* accessions. Through the use of 3,591 densely placed pseudo-landmarks, we were able to predict the accession identity with almost 74% accuracy. The method works well not only on stabilized cultivars, but also on phenotypically more variable wild/feral accessions grown from seed. Unifying the number of leaflets allowed us, for the first time, to make comparisons among several leaves along the main axis, enabling us to investigate developmental changes in leaf shape and detect heterochronic mechanisms influencing the leaf shape in *Cannabis*. The implications of this new high-resolution method in both the cannabis industry and research extend beyond its role in determining *Cannabis* accessions. It also offers a promising tool for developmental studies, and for studying the correlation between leaf shape and phytochemical profiles and the sex of the plants, where lower-resolution methods provided inconclusive results so far. The method presented here offers a fast, effective, robust, and low-cost tool that can aid the future classification of *Cannabis* germplasm. Furthermore, the use of this methodology extends beyond *Cannabis*, and can be applied to numerous other plant species with palmate, pinnate, and lobate leaves with varying numbers of lobes and leaflets where the use of geometric morphometrics methods was not previously possible to this extent.

ACKNOWLEDGEMENTS

This research was supported by projects WECANN (CGL2017-84297-R, Ministerio de Ciencia, Innovación y Universidades), Generalitat de Catalunya (grant number 2021SGR00315) and M. Balant FPI predoctoral contract of the Ministerio de Ciencia, Innovación y Universidades (PRE2018-083226). This work is also supported by NSF Plant Genome Research Program awards IOS-2310355, IOS-2310356, and IOS-2310357. This project was supported by the USDA National Institute of Food and Agriculture, and by Michigan State University

AgBioResearch. We would like to thank Joan Uriach Marsal from Uriach Laboratories for additional financial support. We would also like to acknowledge Cannaflos—Gesellschaft für medizinisches Cannabis mbH for providing seed of accessions IK, IKL and MAR analyzed in the study, Carlos Sáez, Carlos Ribelles, Airy Gras, Joan Vallès, Magsar Urgamal, Shagdar Tsooj, Marine Oganesian and Nina Stepanyan-Gandilyan for help with the sample collection and the cultivation process, and Paula Bruna for helpful advice on improving the quality of scanned images.

COMPETING INTERESTS

None declared.

AUTHOR CONTRIBUTIONS

MB and DHC conceived the study, with OH, TG and DV inputs in a preliminary design phase of the project. MB, TG and DV cultivated the plants. MB and OH selected the method for imaging *Cannabis* leaves. MB and TG scanned the leaves used in the study. MB and DHC developed the morphometric method and MB analyzed the data. MB and DHC wrote the first draft of the paper, that all authors read, commented, and edited.

DATA AVAILABILITY

The datasets and code for the method developed here are freely available on GitHub (https://github.com/BalantM/Cannabis_leaf_morpho_updated, https://github.com/DanChitwood/pinnate_leaf_modeling).

ORCID

Manica Balant https://orcid.org/0000-0002-4316-8511

Teresa Garnatje https://orcid.org/0000-0001-6295-6217

Daniel Vitales https://orcid.org/0000-0002-3109-5028

Oriane Hidalgo https://orcid.org/0000-0002-1547-8627

Daniel H. Chitwood https://orcid.org/0000-0003-4875-1447

SUPPORTING INFORMATION

The datasets and code generated and analyzed in this study are available on GitHub (https://github.com/BalantM/Cannabis_leaf_morpho_updated, https://github.com/DanChitwood/pinnate_leaf_modeling).

REFERENCES

Abràmoff MD, Magalhães PJ, Ram SJ. **2004**. Image processing with ImageJ Part II. *Biophotonics International* **11**: 36–43.

Anderson LC. **1980**. Leaf Variation among *Cannabis* Species from a Controlled Garden. *Botanical Museum leaflets, Harvard University* **28**: 61–69.

Ashby E. **1948**. Studies in the morphogenesis of leaves. I. An essay on leaf shape. *New Phytologist* **47**: 153–176.

Balant M, González Rodríguez R, Garcia S, Garnatje T, Pellicer J, Vallès J, Vitales D, Hidalgo O. **2022**. Novel Insights into the Nature of Intraspecific Genome Size Diversity in *Cannabis sativa* L . *Plants* **11**: 2736.

Biot E, Cortizo M, Burguet J, Kiss A, Oughou M, Maugarny-Calès A, Gonçalves B, Adroher B, Andrey P, Boudaoud A, *et al.* 2016. Multiscale quantification of morphodynamics: MorphoLeaf, software for 2-D shape analysis. *Development* **143**: 3417–3428.

Bookstein FL. **1997**. *Morphometric Tools for Landmark Data: Geometry and Biology*. Cambrige: Cambridge University Press.

Bradski G. **2000**. The OpenCV Library. *Dr. Dobb's Journal: Software Tools for the Professional Programmer* **25**: 120–123.

Bryson AE, Wilson Brown M, Mullins J, Dong W, Bahmani K, Bornowski N, Chiu C, Engelgau P, Gettings B, Gomezcano F, *et al.* 2020. Composite modeling of leaf shape along shoots discriminates *Vitis* species better than individual leaves. *Applications in Plant Sciences* **8**: e11404.

Campbell LG, Peach K, Wizenberg SB. **2021**. Dioecious hemp (*Cannabis sativa* L.) plants do not express significant sexually dimorphic morphology in the seedling stage. *Scientific Reports* **11**: 1–8.

Carlson CH, Stack GM, Jiang Y, Taşklran B, Cala AR, Toth JA, Philippe G, Rose JKC, Smart CD, Smart LB. **2021**. Morphometric relationships and their contribution to biomass and cannabinoid yield in hybrids of hemp (*Cannabis sativa*). *Journal of Experimental Botany* **72**: 7694–7709.

Chen X, Guo H, Zhang Q, Wang L, Guo R, Zhan Y, Lv P, Xu Y, Guo M, Zhang Y, *et al.* 2022. Whole-genome resequencing of wild and cultivated cannabis reveals the genetic structure and adaptive selection of important traits. *BMC Plant Biology* **22**: 371.

Chitwood DH. **2021**. The shapes of wine and table grape leaves: An ampelometric study inspired by the methods of Pierre Galet. *Plants People Planet* **3**: 155–170.

Chitwood DH, Klein LL, O'Hanlon R, Chacko S, Greg M, Kitchen C, Miller AJ, Londo JP. **2016a**. Latent developmental and evolutionary shapes embedded within the grapevine leaf. *New Phytologist* **210**: 343–355.

Chitwood DH, Mullins J, Migicovsky Z, Frank M, VanBuren R, Londo JP. **2021**. Vein-to-blade ratio is an allometric indicator of leaf size and plasticity. *American Journal of Botany* **108**: 571–579.

Chitwood DH, Ranjan A, Martinez CC, Headland LR, Thiem T, Kumar R, Covington MF, Hatcher T, Naylor DT, Zimmerman S, *et al.* 2014. A modern ampelography: A genetic basis for leaf shape and venation patterning in grape. *Plant Physiology* **164**: 259–272.

Chitwood DH, Rundell SM, Li DY, Woodford QL, Yu TT, Lopez JR, Greenblatt D, Kang J, Londo JP. **2016b**. Climate and developmental plasticity: Interannual plasticity in grapevine leaf morphology. *Plant Physiology* **170**: 1480–1491.

Chitwood DH, Sinha NR. **2016**. Evolutionary and Environmental Forces Sculpting Leaf Development. *Current Biology* **26**: R297–R306.

Clarke R, Merlin M. **2013**. Cannabis*: Evolution and ethnobotany*. Berkley, Los Angeles, London: University of California Press.

Demmings EM, Williams BR, Lee C-R, Barba P, Yang S, Hwang C-F, Reisch BI, Chitwood DH, Londo JP. **2019**. Quantitative Trait Locus Analysis of Leaf Morphology Indicates Conserved Shape Loci in Grapevine. *Frontiers in Plant Science* **10**: 1373.

Emboden WA. **1974**. *Cannabis* - a polytypic genus. *Economic Botany* **28**: 304–310.

Failmezger H, Lempe J, Khadem N, Cartolano M, Tsiantis M, Tresch A. **2018**. MowJoe: a method for automated-high throughput dissected leaf phenotyping. *Plant Methods* **14**: 27.

Galet P. **1952**. *Précis d'Ampélographie Pratique*. Digitized by Google Books from Cornell

University.

Galet P, trans. Morton L. **1979**. *A Practical Ampelography: Grapevine Identification*. Cornell University Press (English translation).

Goebel K. **1908**. *Einleitung in die experimentelle Morphologie der Pflanzen*. Leipzig.

Harris CR, Millman KJ, van der Walt SJ, Gommers R, Virtanen P, Cournapeau D, Wieser E, Taylor J, Berg S, Smith NJ, *et al.* 2020. Array programming with NumPy. *Nature* **585**: 357–362.

Hesami M, Pepe M, Jones AMP. **2023**. Morphological Characterization of *Cannabis sativa* L. Throughout Its Complete Life Cycle. *Plants* **12**: 3646.

Heslop-Harrison J, Heslop-Harrison Y. **1958**. Studies on flowering-plant growth and organogenesis-III. Leaf shape changes associated with flowering and sex differentiation in *Cannabis sativa*. *Proceedings of the Royal Irish Academy. Section B: Biological, Geological, and Chemical Science* **59**: 257–283.

Hillig KW. **2004**. A multivariate analysis of allozyme variation in 93 *Cannabis* accessions from the VIR germplasm collection. *Journal of Industrial Hemp* **9**: 5–22.

Hillig KW. **2005a**. A Systematic Investigation of *Cannabis*.

Hillig KW. **2005b**. Genetic evidence for speciation in *Cannabis* (Cannabaceae). *Genetic Resources and Crop Evolution* **52**: 161–180.

Hunter JD. **2007**. Matplotlib: a 2D graphics environment. *Computing in Science and Engineering* **9**: 90–95.

Hurgobin B, Tamiru-Oli M, Welling MT, Doblin MS, Bacic A, Whelan J, Lewsey MG. **2021**. Recent advances in *Cannabis sativa* genomics research. *New Phytologist* **230**: 73–89.

Jin D, Henry P, Shan J, Chen J. **2021a**. Classification of cannabis strains in the Canadian market with discriminant analysis of principal components using genome-wide single nucleotide polymorphisms. *PLOS ONE* **16**: e0253387.

Jin D, Henry P, Shan J, Chen J. **2021b**. Identification of phenotypic characteristics in three chemotype categories in the genus *Cannabis*. *HortScience* **56**: 481–490.

Kuhl FP, Giardina CR. **1982**. Elliptic Fourier features of a closed contour. *Computer Graphics and Image Processing* **18**: 236–258.

Lamarck J-B, Poiret J-L-M. **1783**. *Encyclopédie méthodique. Botanique*. Paris, Panckoucke; Liège, Plomteux.

Lapierre É, Monthony AS, Torkamaneh D. **2023**. Genomics-based taxonomy to clarify

812 cannabis classification. *Genome* **66**: 202–211.
813 **McPartland JM**. **2018**. *Cannabis* Systematics at the Levels of Family, Genus, and Species.
814 *Cannabis and Cannabinoid Research* **3**: 203–212.
815 **McPartland JM, Guy GW**. **2017**. Models of *Cannabis* Taxonomy, Cultural Bias, and Conflicts
816 between Scientific and Vernacular Names. *Botanical Review* **83**: 327–381.
817 **McPartland JM, Small E**. **2020**. A classification of endangered high-THC cannabis (*Cannabis*
818 *sativa* subsp. *indica*) domesticates and their wild relatives. *PhytoKeys* **144**: 81–112.
819 **de Meijer EPM, Keizer LCP**. **1996**. Patterns of diversity in *Cannabis*. *Genetic Resources and*
820 *Crop Evolution* **43**: 41–52.
821 **Migicovsky Z, Swift JF, Helget Z, Klein LL, Ly A, Maimaitiyiming M, Woodhouse K, Fennell**
822 **A, Kwasniewski M, Miller AJ, *et al.* 2022**. Increases in vein length compensate for leaf area
823 lost to lobing in grapevine. *American Journal of Botany* **109**: 1063–1073.
824 **Moliterni VMC, Cattivelli L, Ranalli P, Mandolino G**. **2004**. The sexual differentiation of
825 *Cannabis sativa* L.: A morphological and molecular study. *Euphytica* **140**: 95–106.
826 **Murovec J, Eržen JJ, Flajšman M, Vodnik D**. **2022**. Analysis of Morphological Traits,
827 Cannabinoid Profiles, THCAS Gene Sequences, and Photosynthesis in Wide and Narrow
828 Leaflet High-Cannabidiol Breeding Populations of Medical Cannabis. *Frontiers in Plant*
829 *Science* **13**: 786161.
830 **Naim-Feil E, Pembleton LW, Spooner LE, Malthouse AL, Miner A, Quinn M, Polotnianka**
831 **RM, Baillie RC, Spangenberg GC, Cogan NOI**. **2021**. The characterization of key physiological
832 traits of medicinal cannabis (*Cannabis sativa* L.) as a tool for precision breeding. *BMC Plant*
833 *Biology* **21**: 1–15.
834 **Niklas KJ**. **1994**. *Plant allometry: the scaling of form and process*. Chicago: University of
835 Chicago Press.
836 **Pedregosa F, Varoquaux G, Gramfort A, Michel V, Thirion B, Grisel O, Blondel M,**
837 **Prettenhofer P, Weiss R, Dubourg V, *et al.* 2011**. Scikit-learn: Machine Learning in Python.
838 *Journal ofMachine Learning Research* **12**: 2825–2830.
839 **Potter DJ**. **2009**. *Optimisation Of* Cannabis sativa *L. As A Phytopharmaceutical [PhD Thesis]*.
840 London: King's College London, Department of Pharmaceutical Science Research.
841 **Prentout D, Razumova O, Rhoné B, Badouin H, Henri H, Feng C, Käfer J, Karlov G, Marais**
842 **GAB**. **2020**. An efficient RNA-seq-based segregation analysis identifies the sex chromosomes
843 of *Cannabis sativa*. *Genome Research* **30**: 164–172.

844 **Quimby MW, Doorenbos NJ, Turner CE, Masoud A**. **1973**. Mississippi-Grown Marihuana -
845 *Cannabis sativa* Cultivation and Observed Morphological Variations. *Economic Botany* **27**:
846 117–127.
847 **Ravaz L**. **1902**. *Les vignes américaines: Porte-greffes et producteurs directs*. Goulet,
848 Montpellier and Paris: Digitized by Google Books from Cornell University.
849 **Ren G, Zhang X, Li Y, Ridout K, Serrano-Serrano ML, Yang Y, Liu A, Ravikanth G, Nawaz MA,**
850 **Mumtaz AS, *et al.* 2021**. Large-scale whole-genome resequencing unravels the
851 domestication history of *Cannabis sativa*. *Science Advances* **7**: eabg2286.
852 **Sawler J, Stout JM, Gardner KM, Hudson D, Vidmar J, Butler L, Page JE, Myles S**. **2015**. The
853 Genetic Structure of Marijuana and Hemp. *PLOS ONE* **10**: e0133292.
854 **Schultes RE, Klein WM, Plowman T, Lockwood TE**. **1974**. *Cannabis*: An example of
855 taxonomic neglect. *Botanical Museum Leaflets, Harvard University* **23**: 337–367.
856 **Schwabe AL, McGlaughlin ME**. **2019**. Genetic tools weed out misconceptions of strain
857 reliability in *Cannabis sativa*: implications for a budding industry. *Journal of Cannabis*
858 *Research* **1**: 3.
859 **Small E**. **2015**. Evolution and Classification of *Cannabis sativa* (Marijuana, Hemp) in Relation
860 to Human Utilization. *Botanical Review* **81**: 189–294.
861 **Small E, Beckstead HD**. **1973**. Cannabinoid Phenotypes in *Cannabis sativa*. *Nature* **245**: 147–
862 148.
863 **Small E, Cronquist A**. **1976**. A Practical and Natural Taxonomy for *Cannabis*. *Taxon* **25**: 405–
864 435.
865 **Small E, Jui PY, Lefkovitch LP**. **1976**. A Numerical Taxonomic Analysis of *Cannabis* with
866 Special Reference to Species Delimitation. *Systematic Botany* **1**: 67–84.
867 **Spitzer-Rimon B, Duchin S, Bernstein N, Kamenetsky R**. **2019**. Architecture and Florogenesis
868 in Female *Cannabis sativa* Plants. *Frontiers in Plant Science* **10**: 350.
869 **Spitzer-Rimon B, Shafran-Tomer H, Gottlieb GH, Doron-Faigenboim A, Zemach H,**
870 **Kamenetsky-Goldstein R, Flaishman M**. **2022**. Non-photoperiodic transition of female
871 cannabis seedlings from juvenile to adult reproductive stage. *Plant Reproduction* **35**: 265–
872 277.
873 **Stack GM, Toth JA, Carlson CH, Cala AR, Marrero-González MI, Wilk RL, Gentner DR,**
874 **Crawford JL, Philippe G, Rose JKC, *et al.* 2021**. Season-long characterization of high-
875 cannabinoid hemp (*Cannabis sativa* L.) reveals variation in cannabinoid accumulation,

876 flowering time, and disease resistance. *GCB Bioenergy* **13**: 546–561.
877 **Terpilowski M**. **2019**. scikit-posthocs: Pairwise multiple comparison tests in Python. *Journal*
878 *of Open Source Software* **4**: 1169.
879 ***The Global Cannabis Report, 3rd Edition***. **2022**. London, Berlin, Barcelona: Prohibition
880 Partners.
881 **Torres A, Pauli C, Givens R, Argyris J, Allen K, Monfort A, Gaudino RJ**. **2022**.
882 High-throughput methods to identify male *Cannabis sativa* using various genotyping
883 methods. *Journal of Cannabis Research* **4**: 57.
884 **Toth JA, Stack GM, Cala AR, Carlson CH, Wilk RL, Crawford JL, Viands DR, Philippe G, Smart**
885 **CD, Rose JKC, *et al.* 2020**. Development and validation of genetic markers for sex and
886 cannabinoid chemotype in *Cannabis sativa* L. *GCB Bioenergy* **12**: 213–222.
887 **Vergara D, Feathers C, Huscher EL, Holmes B, Haas JA, Kane NC**. **2021**. Widely assumed
888 phenotypic associations in *Cannabis sativa* lack a shared genetic basis. *PeerJ* **9**: e10672.
889 **Virtanen P, Gommers R, Oliphant TE, Haberland M, Reddy T, Cournapeau D, Burovski E,**
890 **Peterson P, Weckesser W, Bright J, *et al.* 2020**. SciPy 1.0: fundamental algorithms for
891 scientific computing in Python. *Nature Methods* **17**: 261–272.
892 **Watts S, McElroy M, Migicovsky Z, Maassen H, van Velzen R, Myles S**. **2021**. *Cannabis*
893 labelling is associated with genetic variation in terpene synthase genes. *Nature Plants* **7**:
894 1330–1334.
895 **Zhukovskii PM**. **1971**. *Cultivated plants and their wild relatives*. Leningrad, USSR, Kolos.
896